Available online at www.sciencedirect.com
ScienceDirect
Bioorganic & Medicinal Chemistry 16 (2008) 5881–5889
Bioorganic & Medicinal Chemistry

Towards the first inhibitors of trihydroxynaphthalene reductase from *Curvularia lunata*: Synthesis of artificial substrate, homology modelling and initial screening

Mojca Brunskole,[a] Bogdan Štefane,[b] Karmen Zorko,[c] Marko Anderluh,[c] Jure Stojan,[a] Tea Lanišnik Rižner[a] and Stanislav Gobec[c,*]

[a]*Institute of Biochemistry, Faculty of Medicine, University of Ljubljana, Vrazov trg 2, 1000 Ljubljana, Slovenia*
[b]*Faculty of Chemistry and Chemical Technology, University of Ljubljana, Aškerčeva 5, 1000 Ljubljana, Slovenia*
[c]*Faculty of Pharmacy, University of Ljubljana, Aškerčeva 7, 1000 Ljubljana, Slovenia*

Received 11 March 2008; revised 19 April 2008; accepted 25 April 2008
Available online 29 April 2008

Dedicated to Professor Slavko Pečar on the occasion of his 60th birthday

Abstract—Trihydroxynaphthalene reductase (3HNR) is an essential enzyme in the biosynthesis of fungal melanin and it represents an emerging target for the development of new fungicides and antimicotics. To promote the discovery of new inhibitors, an improved chemical synthesis of the artificial substrate 2,3-dihydro-2,5-dihydroxy-4*H*-benzopyran-4-one (DDBO) was developed. A series of compounds were screened on 3HNR from *Curvularia lunata*, a known plant pathogen and an opportunistic human pathogen, and several structurally diverse hits were obtained. Homology modelling of 3HNR from *C. lunata* can explain their binding modes and will enable further structure-based design of new and improved inhibitors.

1. Introduction

Dematiaceous, or darkly pigmented, fungi are responsible for life-threatening infections in both immunocompromised and immunocompetent individuals.[1] They are the main causative agents of phaeohyphomycosis, chromoblastomycosis and eumycotic micetoma, with clinical manifestations including local infections, allergic diseases, pneumonia, keratitis, brain abscess and disseminated infections.[1–3] Disseminated phaeohyphomycosis is a relatively rare infection that is caused by pigmented fungi; however, the incidence of this mycosis has been increasing in recent years.[4] The outcome for antifungal therapy is still very poor, with an overall mortality rate of 79% despite combined antimicotic treatments and surgical excision of the infected area.[4] Dematiaceous fungi are distributed throughout the World, but the majority of patients with phaeohyphomycosis are from North America and Europe.[4] Growing incidences of fungal infections and progressive antifungal drug resistance indicate the need for the development of new and more potent antimicotics with new mechanisms of action.

Melanin protects pigmented fungi against environmental stresses and host defence mechanisms.[5] It has been shown that melanization protects the pathogenic fungi *Cryptococcus neoformans*, *Sporothrix schenckii*, *Fonsecaea pedrosoi*, *Aspergillus fumigatus* and *Exophiala dermatitidis* against the mammalian immune system, oxidative burst and phagocytosis.[6] Melanins thus have important roles in the virulence and pathogenicity of these pathogenic fungi.[5] Although different types of fungal melanin exist, numerous plant and human pathogenic fungi synthesize their melanins from dihydroxynaphthalene and related pentaketide metabolites.[5] The synthesis of 1,8-dihydroxynaphthalene (DHN)-melanin begins with polyketide synthase, which links acetate units to produce 1,3,6,8-tetrahydroxynaphthalene (4HN) (Fig. 1). A tetrahydroxynaphthalene reductase then reduces 4HN to scytalone, which is converted to 1,3,8-trihydroxynaphthalene (3HN) by scytalone dehydratase. This is followed by the reduction of 3HN to vermelone by trihydroxynaphthalene reductase

Keywords: Melanin biosynthesis inhibitors; Antifungal drugs; Fungicides.
* Corresponding author. Tel.: +386 1 4769585; fax: +386 1 4258031; e-mail: gobecs@ffa.uni-lj.si

0968-0896/$ - see front matter © 2008 Elsevier Ltd. All rights reserved.
doi:10.1016/j.bmc.2008.04.066

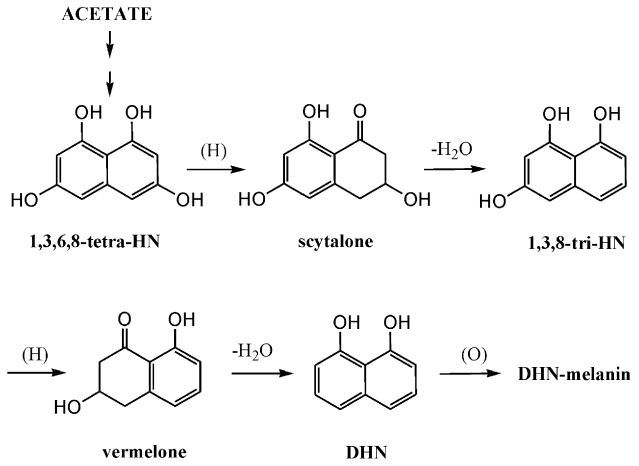

Figure 1. 1,8-Dihydroxynaphthalene (DHN)-melanin biosynthesis in *C. lunata* (1,3,6,8-tetra-HN: 1,3,6,8-tetrahydroxynaphthalene; 1,3,8-tri-HN: 1,3,8-trihydroxynaphthalene).

(3HNR) and dehydration of vermelone to DHN by vermelone dehydratase. DHN-melanin is formed by enzymatic polymerization.[7] With melanin having an important role in fungal pathogenicity, these enzymes participating in its biosynthesis represent attractive targets for the development of new fungicides and antimicotics. Moreover, since the DHN-melanin biosynthetic pathway does not exist in off-target organisms, a selective activity can be achieved.

Inhibitors of melanin biosynthesis have mostly been studied in the fungal rice-blast pathogen *Magnaporthe grisea*.[8,9] Rice-blast disease represents an enormous economic problem because of annual reductions in crop yields.[10] Commercially available agents for preventing this crop disease target 3HNR (tricyclazole, pyroquilon and phthalide) and scytalone dehydratase (carpropamid) (Fig. 2).[7,11] All the inhibitors of melanin biosynthesis in use are fungicides, and currently there are no antimicotics available that would target these enzymes.

Curvularia lunata is a melanized filamentous fungus that is found primarily in soil. It is a known plant and human pathogen,[12,13] and is the causative agent of infections characteristic of dark pigmented fungi. In *C. lunata*, melanin is produced via the pentaketide pathway, from

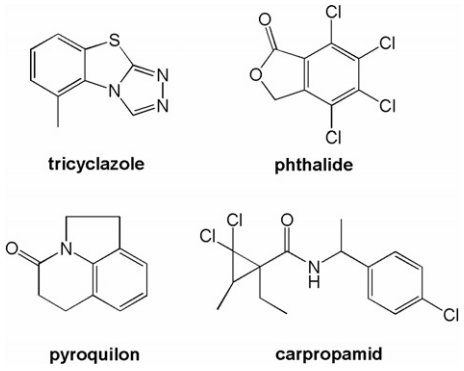

Figure 2. Fungicides that target the melanin biosynthetic pathway by inhibiting 3HNR (tricyclazole, pyroquilon, phthalide) and scytalone dehydratase (carpropamid).

DHN.[14] 3HNR from *C. lunata* has recently been cloned and expressed in *Escherichia coli*.[14] Here, we have investigated 3HNR from *C. lunata* as a potential target for inhibition of the melanin biosynthetic pathway. Initially there were two problems. First, because 3HNR has not been crystallized yet, we had to predict its structure by homology modelling, with the intention of studying the features of 3HNR and its active site, with a view to the structure-based discovery of inhibitors. Second, the physiological substrate of 3HNR, 3HN, is not stable in aerated solutions, as it rapidly oxidizes.[15] It is thus inappropriate for in vitro enzymatic assays. Since we could not repeat the synthesis of the non-physiological substrate 2,3-dihydro-2,5-dihydroxy-4*H*-benzopyran-4-one (DDBO) as published by Thompson et al.,[15] we had to find an alternative synthesis that would provide us with sufficient amounts of DDBO for biochemical evaluation of 3HNR inhibitors. In addition, our in-house bank of compounds was screened for inhibition of 3HNR, with initial hits being discovered that inhibited 3HNR in the micromolar range.

2. Results and discussion

2.1. Synthesis

The detailed synthesis of 2,3-dihydro-2,5-dihydroxy-4*H*-chromen-4-one (**6**) is depicted in Scheme 1. Although the synthesis of **6** had been described earlier by Thompson et al.,[15] we were not able to repeat this synthesis in our laboratories. The major problems were incomplete benzylation of the resorcinolic functionality of compound **1**, and the formation of a complex reaction mixture during the condensation of dibenzyl ether **3** with ethyl formate under the reaction conditions described. Consequently, we modified the above-mentioned strategy towards the target 4*H*-chromen-4-one **6**. First, a variety of reaction conditions were tried to benzylate both of the phenolic functional groups of compound **1** in a single step; unfortunately, in all cases, we obtained a mixture of mono- and dibenzylated products which were difficult to separate. Accordingly, complete protection was achieved via a stepwise procedure using benzyl bromide in the presence of K_2CO_3, to obtain the monobenzylated product **2**, and in the second step a NaH/BnBr system was used to benzylate the second hydroxylic group (Scheme 1). With this dibenzyl intermediate **3** in our hands, we then focused our attention on the production of 3-oxo-3-phenylpropanal **5**. The method described by Thompson et al.[15] using methyl formate and sodium hydride in DMF again appeared to be problematic. Even with the screening of a variety of different reaction conditions, complex reaction mixtures were formed, as indicated by ^{1}H NMR spectra. For this reason, we attempted the formation of the 1,3-ketoaldehyde moiety in **5** through the *N*,*N*-dimethylamine derivative **4**, which should subsequently undergo hydrolysis to form the desired 1,3-ketoaldehyde **5**. However, as shown in Scheme 1, when the *N*,*N*-dimethylamine derivative **4** was treated under carefully controlled hydrolytic conditions, a retroaldol reaction occurred, producing only the starting dialkoxyacetophe-

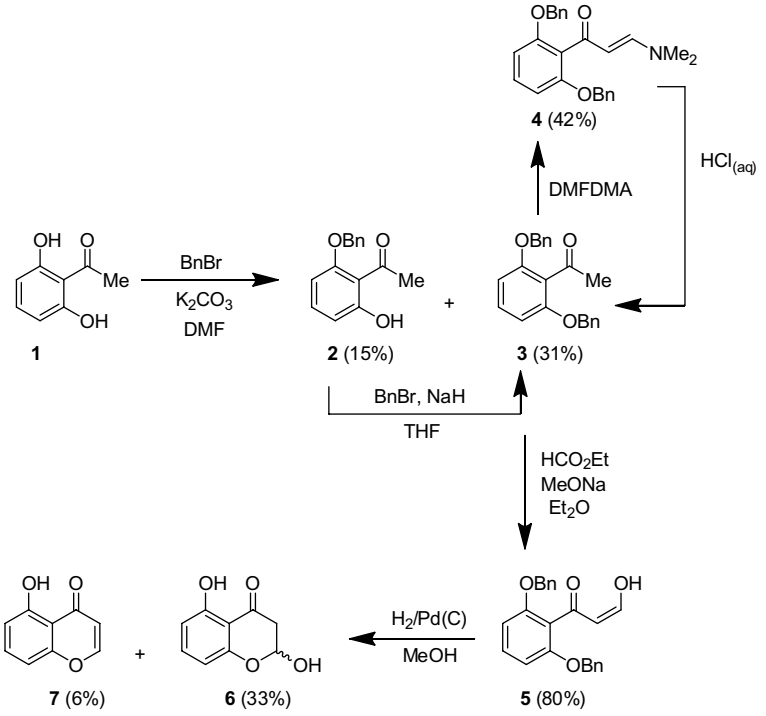

Scheme 1. Synthesis of 2,3-dihydro-2,5-dihydroxy-4*H*-chromen-4-one.

none **3**. Subsequently, we searched for better formylating conditions to obtain the desired 1,3-ketoaldehyde moiety. Fortunately, we found that formylation works well in diethyl ether using ethyl formate and sodium methoxide as a base, producing **5** in a good yield. It is worth mentioning here that only the enol tautomer form of compound **5** was indicated by ^{1}H NMR spectra of the pure product in chloroform solution. The final step was the reduction of **5** under catalytic hydrogenation conditions, resulting in the formation of 2,3-dihydro-2,5-dihydroxy-4*H*-chromen-4-one (**6**) (33%) and its dehydrated analogue **7** (6%). The hemiacetal moiety of the 4*H*-chromen-4-one derivative **6** was found to be sensitive to basic conditions, such as the presence of Et_3N or Na_2CO_3, resulting in the quantitative formation of **7**.

2.2. Homology modelling

Prior to this study, structure-based methods could not be used for the discovery of inhibitors of 3HNR from *C. lunata* because the experimental structure of the enzyme was not available. Here, we created the homology model of 3HNR from *C. lunata* with a docked DDBO. This was achieved according to the solved structure of 3HNR from *M. grisea*,[16] with which 3HNR from *C. lunata* shares 74% sequence identity, with only one insertion of two amino acids and one deletion of a single amino acid (Fig. 3). As a template, we also included some aspects from the solved structure of 17β-HSDcl[17] in the modelling, which possesses 58% identical residues and lacks the same two amino acids in a peripheral loop near the N-terminal. As expected for such a high homology model, it was very stable during the extensive dynamic simulation, with a good quality score at the end (PROCHECK).[18] Moreover, over their entire backbone,

```
  1 - 50  DAIPGPLGPQSASLEGKVALVTGAGRGIGREMAMELGRRGCKVIVNYANS
                  *  ** **** *** *****  ** **  ** ** *****
  1 - 50  ----MANIEQTWSLAGKVAVVTGSGRGIGKAMAIELAKRGAKVAVNYANA

 51 - 100 TESAEEVVAAIKK--NGSDAACVKANVGVVEDIVRMFEEAVKIFGKLDIV
           * ** **  **   *****   ***** **          ** ******
 51 - 100 VEGAEQVVKEIKALNNGSDAHAFKANVGNVEESEKLMDDVVKHFGKLDIC

101 - 150 CSNSGVVSFGHVKDVTPEEFDRVFTINTRGQFFVAREAYKHLEIGGRLIL
           ********** ************ **********  ***  *  ** **
101 - 150 CSNSGVVSFGHFKDVTPEEFDRVFNINTRGQFFVAKAAYKRMENYGRIIL

151 - 200 MGSITGQAKAVPKHAVYSGSKGAIETFARCMAIDMADKKITVNVVAPGGI
           ********* ***************** ******   ****** ******
151 - 200 MGSITGQAKGVPKHAVYSGSKGAIETFTRCMAIDAGEKKITVNCVAPGGI

201 - 250 KTDMYHAVCREYIPNGENLSNEEVDEYAAVQWSPLRRVGLPIDIARVVCF
           ************** ** **   *****   ***  *** * ********
201 - 250 KTDMYHAVCREYIPGGEKLSDDQVDEYACT-WSPHNRVGQPVDIARVVCF

251 - 272 LASNDGGWVTGKVIGIDGGACM
           *** ** ** ******** ***
251 - 272 LASQDGEWVNGKVIGIDGAACM
```

Figure 3. Comparison of the amino-acid sequences of 3HNR from *M. grisea* (top line) and *C. lunata* (bottom line), with residues 14–283 seen in the X-ray structure of 3HNR from *M. grisea* (chain A in 1YBV) shown. Asterisks denote the identical residues (74%).

the RMS between the final frame (see Section 4.2) of 3HNR from the *C. lunata* model and the template crystal structure of 3HNR from *M. grisea* was only 0.75 Å.

This homology model was used for docking studies to determine the binding mode of our initial inhibitors (see 2.4.). In addition, the comparative model of 3HNR from *C. lunata* can now be used for structure-based virtual high-throughput screening (VHTS) efforts. Although docking and VHTS using comparative models are more challenging and less successful than docking to crystallographic structures,[19] many protein models have recently been used in this way to aid inhibitor design.[20,21]

Figure 4 shows the docked DDBO in the active site of 3HNR from *C. lunata*. It is sandwiched between the pyridine ring of $NADP^+$ and the phenol ring of Tyr208 (Tyr223 in 3HNR from *M. grisea*). Its hemiacetal hydroxyl group in the beta position is pointing into the space between the hydroxyl groups of Ser149 and Tyr163 of the catalytic triad, whilst the corresponding hydrogen is ready for transfer to C4 of the pyridine ring. Although we docked DDBO according to the position of dihydroxyphenyl dihydroxy dihydro chromenone in the active site of grape dihydroflavonol 4-reductase (PDB code 2NNL),[22] it should be stressed that we could have also used tricyclazole (PDB code 1YBV), piroquilon (PDB code 1G0O) or 4-nitro-inden-1-one (PDB code 1DOH) as reference positions. Namely, they are all approximately of the same size as DDBO, and there is just enough space for them to be accommodated in front of the Ser149 and Tyr163.

Finally, there is the question as to whether modelling can suggest the mechanism of DDBO reduction by 3HNR from *C. lunata*. As a higher pH is favourable for the reaction, it would be expected that hydroxyl ions are a direct, or more likely an indirect, proton acceptor. A plausible pathway is via deprotonated Tyr163. However, a water molecule coordinated between Ser149, Tyr208 and His160 might also participate in the proton transfer from the hemiacetal hydroxyl group of DDBO. This latter explanation is consistent with the observation of Liao et al.[23] that as compared to wild-type 3HNR, an H175A mutant of 3HNR from *M. grisea* (His160 in 3HNR from *C. lunata*) loses more than 90% of its activity.

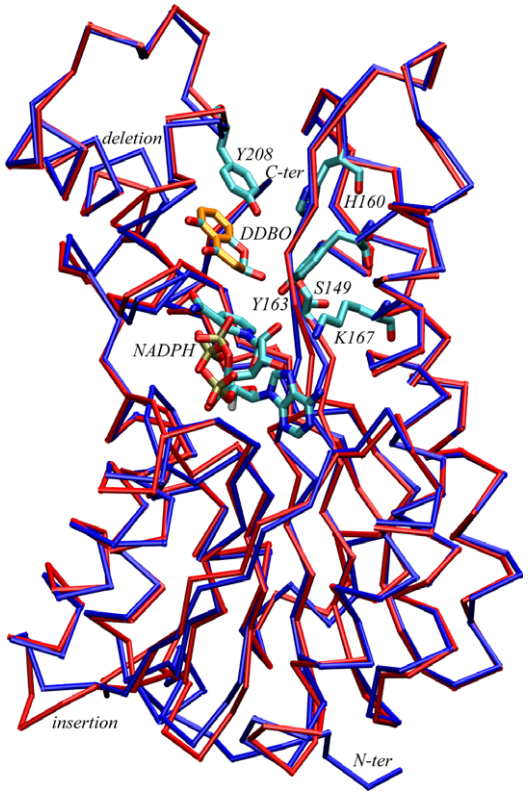

Figure 4. Backbone tracing of the homology built model (red) of 3HNR from the fungus *C. lunata* superimposed on the template X-ray structure of 3HNR from *M. grisea* (blue). The RMS of the two backbone chain atoms is 0.75 Å. Note the catalytic triad residues S149/Y163/K167, the two residues at the entrance to the active site (Y208/H160), the coenzyme NADPH and the substrate DDBO. The positions of an insertion (two amino acids) at the N-terminal and a deletion (one amino acid) at the C-terminal are also indicated.

2.3. Compound screening

With the recombinant 3HNR enzyme from *C. lunata* purified to homogeneity, this enabled an evaluation of potential inhibitors by a fast spectrophotometric assay. We have examined the inhibitory potential of several groups of compounds from our in-house collection that were selected based on their structural similarities to the natural and artificial substrates that are known inhibitors of 3HNR from the fungus *M. grisea* and inhibitors of other oxido-reductive enzymes of interest. More than 100 compounds were screened. The best inhibitors were some non-steroidal anti-inflammatory drugs (NSAIDs), 1,3-indandion and two compounds with a chromen-4-on[24] scaffold (Table 1).

Table 1. Inhibitors of recombinant 3HNR from *C. lunata*

Compound	Structure	IC_{50} (μM)
8 (Etodolac)	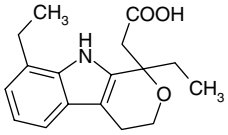	17
9	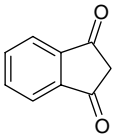	66
10 (Diclofenac)	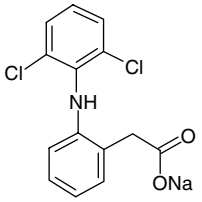	108
11 (Nabumetone)	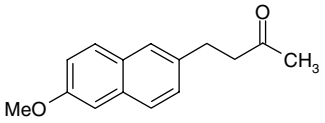	111
12	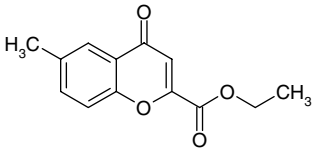	120
13	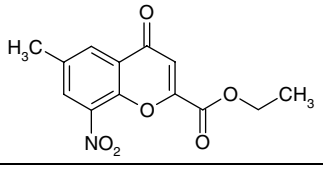	167

Amongst these NSAIDs, etodolac (**8**) was the most potent inhibitor (IC_{50} = 17 μM), followed by diclofenac (**10**, IC_{50} = 108 μM) and nabumetone (**11**, IC_{50} = 111 μM). Also celecoxib and naproxen showed modest inhibitory activities (17% and 9% inhibitions, respectively), whilst phenacetin, ibuprofen, ketoprofen and paracetamol did not inhibit 3HNR (data not shown). From the series of compounds with indan, indol, 1,4-benzoxazine and benzimidazole scaffolds, only 1,3-indandion (**9**) revealed promising activity, with an IC_{50} of 66 μM. Amongst the compounds with a chromen-4-on structure, ethyl esters **12** and **13** showed promising inhibition, with IC_{50} values below 200 μM. Here, introduction of a nitro group or larger substituent at position 8 decreased the inhibitory effects.

2.4. Docking studies

To explain the binding modes of the most potent of the inhibitors obtained, a docking study with the comparative model of 3HNR from *C. lunata* was performed using AutoDock 3.0. The ranking of docking scores for compounds **8** and **9** (calculated final docked energies were −11.9 kcal/mol and −6.65 kcal/mol, respectively) correlates with experimental 3HNR inhibition values where etodolac (**8**) is better inhibitor than 1,3-indandion (**9**). Simulations revealed that these inhibitors can enter the substrate-binding region of the active site. In the arrangements with the lowest docked energies, compounds **8** and **9** were sandwiched between the pyridine ring of the NADPH coenzyme and the phenol ring of Tyr208 (Figs. 5 and 6). One of the carbonyl groups of compound **9** was oriented towards the hydroxyl groups of the catalytic amino-acid residues Ser149 and Tyr163. The positions of selected inhibitors within the active site of 3HNR from *C. lunata* are similar to the positions of commercially available and other inhibitors within the active site of 3HNR from *M. grisea*, as published by Jordan et al.[8]

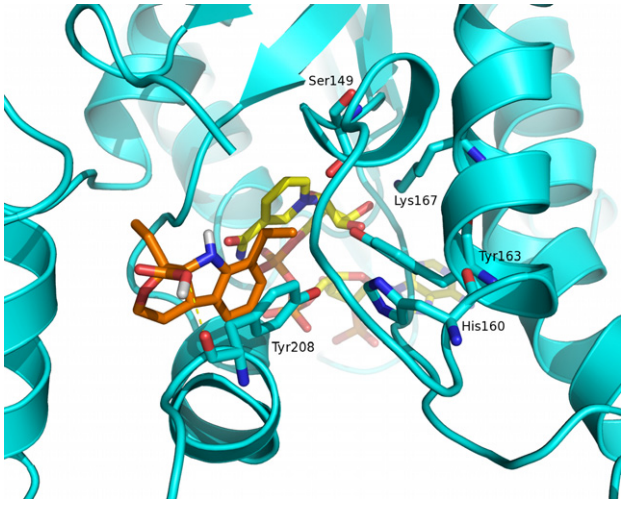

Figure 5. Docking of compound **8** (orange) into the active site of 3HNR from *C. lunata*. The coenzyme NADPH (yellow) is also shown, along with the amino-acid residues of the catalytic triad: Ser149, Tyr163 and Lys167, and two amino-acid residues at the entrance to the active site: His160 and Tyr208 (all in blue).

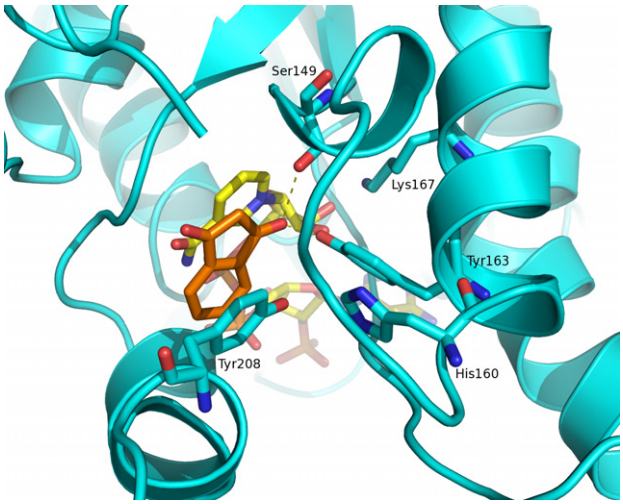

Figure 6. Docking of compound **9** (orange) into the active site of 3HNR from *C. lunata*. Details as given for Figure 5.

3. Conclusions

To conclude, we have presented here an improved synthesis of an artificial substrate of 3HNR, an enzyme that is involved in the biosynthesis of fungal melanin and that represents an important target for the development of new fungicides and antifungal drugs. With the screening of our in-house library of compounds, we have identified the initial structurally diverse hits. To enable the rational structure-based design of new and more potent inhibitors, a homology built model of 3HNR from *C. lunata* was constructed.

4. Experimental

4.1. Chemistry

4.1.1. General. Solvents and starting compounds were obtained from commercial sources (Fluka, Sigma and Aldrich). All reactions were carried out in dry solvents. Light petroleum refers to the fraction with the boiling point of 40–60 °C. TLC was carried out on Fluka silica-gel TLC cards. All melting points were determined on a hot stage apparatus and are uncorrected. IR spectra were recorded on a BioRad FTS 3000MX instrument. NMR spectra were recorded on a Bruker Avance 300 DPX spectrometer at 302 °C. Chemical shifts are reported in δ ppm, referenced to an internal TMS standard for ^{1}H NMR, chloroform-*d* (δ 77.0), DMSO-d_6 (δ 39.5) for ^{13}C NMR. The ^{1}H–^{13}C HMBC spectra were obtained with 512 time increments and 32 scans per t_1 increment. Microanalyses were performed on a Perkin-Elmer 2400 series II CHNS/O analyzer. Mass spectra and high-resolution mass measurements were performed on a VG-Analytical Autospec EQ instrument.

4.1.2. 1-[2,6-Bis(benzyloxy)phenyl]ethanone (3). To a solution of 1-(2,6-dihydroxyphenyl)ethanone (**1**) (6.09 g, 40 mmol) and K_2CO_3 (55.80 g, 0.40 mol) in DMF (300 mL), BnBr (27.40 g, 0.16 mol) was added.

The resulting suspension was heated to 80 °C for 3 h. After the reaction was complete, the mixture was filtered and concentrated under reduced pressure. The residue was dissolved in EtOAc (250 mL) and washed with H_2O (3× 100 mL) and brine (2× 100 mL). The organic phase was dried (Na_2SO_4) and evaporated under reduced pressure, and the residue was purified by column chromatography (petroleum ether/EtOAc, 10:1) to give the mono- and dibenzylated products, at 1.46 g (15%) and 4.09 g (31%), respectively. 1-[2-(Benzyloxy)-6-hydroxyphenyl]ethanone (**2**) (1.40 g, 5.79 mmol) was then dissolved in THF (30 mL). After the subsequent addition of NaH (60%, 255 mg, 6.37 mmol) and BnBr (4.95 g, 28.95 mmol), the reaction mixture was stirred at room temperature for 48 h. The reaction mixture was then diluted with EtOAc (100 mL) and washed with H_2O (2× 100 mL) and brine (100 mL) before being dried (Na_2SO_4), and evaporated under reduced pressure. The residue was dissolved in Et_2O (30 mL), treated with pyridine (10 mL) and left at room temperature for 8 h. The precipitated material was filtered off and washed with Et_2O (2× 30 mL). The mother liquid was washed with HCl (5%, 2× 30 mL) and brine (30 mL), and then dried over Na_2SO_4 and evaporated under reduced pressure. The residue, yellowish solid, was recrystallized from the solvent mixture (Et_2O/petroleum ether) to give the dibenzylated product **3** as a white solid, at 1.60 g (83%). 1-[2-(Benzyloxy)-6-hydroxyphenyl]ethanone (**2**): R_f 0.54 (petroleum ether/EtOAc, 5:1); mp 105–107 °C (109–110 °C)[25]; IR (ν_{max}/cm^{-1}, KBr) 3410, 1626, 1594, 1452, 1362, 1233, 1074, 851, 784, 756, 711, 640; ^{1}H NMR (300 MHz, $CDCl_3$) δ 2.62 (s, 3H), 5.13 (s, 2H), 6.47 (d, 1H, J = 8.5 Hz), 6.59 (dd, 1H, J = 8.5, 1.0 Hz), 7.32 (dd, 1H, J = 8.5, 8.5 Hz), 7.35–7.44 (m, 5H), 13.23 (s, 1H); ^{13}C NMR (75 MHz, $CDCl_3$) δ 34.0, 71.1, 102.2, 111.0, 111.5, 127.9, 128.4, 128.7, 135.8, 136.0, 160.6, 164.7, 205.1; MS (EI, 70 eV, *m*/*z*, (%)) 242 (M$^+$, 11), 91 (100); HRMS (EI) *m*/*z* calcd for $C_{15}H_{14}O_3$: 242.0943; found: 242.0950. 1-[2,6-Bis(benzyloxy)phenyl]ethanone (**3**): R_f 0.30 (petroleum ether/EtOAc, 5:1); mp 68–70 °C (68.5–70 °C)[26]; IR (ν_{max}/cm^{-1}, KBr) 1705, 1592, 1451,1355, 1269, 1232, 1107, 775, 733, 695; ^{1}H NMR (300 MHz, $CDCl_3$) δ 2.55 (s, 3H), 5.12 (s, 4H), 6.65 (d, 2H, J = 8.5 Hz), 7.23 (dd, 1H, J = 8.5, 8.5 Hz), 7.31–7.46 (m, 10H); ^{13}C NMR (75 MHz, $CDCl_3$) δ 32.3, 70.4, 105.8, 121.8, 127.0, 127.8, 128.5, 130.4, 136.6, 155.7, 202.2; MS (EI, 70 eV, *m*/*z*, (%)) 332 (M$^+$, 0.5%), 91 (100); HRMS (EI) *m*/*z* calcd for $C_{22}H_{20}O_3$: 332.1413; found: 332.1421.

4.1.3. 1-[2,6-Bis(benzyloxy)phenyl]-3-(dimethylamino) prop-2-en-1-one (4). A mixture of 1-[2,6-bis(benzyloxy)phenyl]ethanone (**3**) (673 mg, 2.03 mmol) and DMFDMA (482 mg, 4.05 mmol) in THF (5 mL) was heated under reflux for 4 h. The solvent was then evaporated under reduced pressure, and the residue purified by column chromatography (petroleum ether/EtOAc, 1:1) to give dimethylamino derivate **4** as a yellowish solid, at 329 mg (42%). R_f 0.11 (petroleum ether/EtOAc, 1:1); mp 71–74 °C; IR (ν_{max}/cm^{-1}, KBr) 3032, 1734, 1591, 1451, 1384, 1308, 1258, 1100, 1072, 900, 741; ^{1}H NMR (300 MHz, $CDCl_3$) δ 2.88 (s, 6H), 5.13 (s, 4H), 5.41 (d, 1H, J = 13.0 Hz), 6.59 (d, 2H, J = 8.5 Hz), 7.13 (dd, 1H, J = 8.5, 8.5 Hz), 7.24–7.42 (m, 11H); ^{13}C NMR (75 MHz, $CDCl_3$). δ 36.8, 44.4, 70.2, 100.4, 106.2, 121.9, 126.7, 127.3, 128.1, 129.0, 137.2, 155.0, 190.5; MS (EI, 70 eV, *m*/*z*, (%)) 387 (M$^+$, 4%), 91 (100); HRMS (EI) *m*/*z* calcd for $C_{25}H_{25}NO_3$: 387.1834, found: 387.1840; Anal. Calcd for $C_{25}H_{25}NO_3$: C, 77.49; H, 6.50; N, 3.69; found: C, 77.72; H, 6.45; N, 3.63.

4.1.4. 3-[2,6-Bis(benzyloxy)phenyl]-3-oxopropanal (5). MeONa (407 mg, 7.53 mmol) was suspended in dry Et_2O (20 mL), and a solution of 1-[2,6-bis(benzyloxy)phenyl]ethanone (**3**) (2.00 g, 6.02 mmol) and HCO_2Et (1.115 g, 15.05 mmol) in dry Et_2O (10 mL) was added. The reaction mixture was stirred at room temperature for 4 h and then treated with H_2O (30 mL). The layers were separated and the aqueous phase was washed with Et_2O (30 mL), acidified with HCl (5%, 9.6 mL) and extracted with Et_2O (6× 90 mL). The combined organic phases were washed with H_2O (250 mL), and dried (Na_2SO_4) and evaporated under reduced pressure to give 1.74 g (80%) of pure product **5**. R_f 0.17 (petroleum ether/EtOAc, 5:1); mp 71–74 °C; IR (ν_{max}/cm^{-1}, KBr) 3028, 1622, 1593, 1470, 1377, 1290, 1256, 1099, 1016, 903, 846, 797, 737, 697; ^{1}H NMR (300 MHz, $CDCl_3$) δ 5.14 (s, 4H), 5.85 (d, 1H, J = 4.5 Hz), 6.64 (d, 2H, J = 8.5 Hz), 7.25 (dd, 1H, J = 8.5, 8.5 Hz), 7.20–7.42 (m, 10H), 7.92 (d, 1H, J = 4.5 Hz), 14.57 (br s, 1H); ^{13}C NMR (75 MHz, $CDCl_3$) δ 70.5, 106.1, 118.1, 126.8, 127.2, 127.7, 128.5, 131.3, 136.7, 156.7, 173.6, 191.6; MS (EI, 70 eV, *m*/*z*, (%)) 360 (M$^+$, 0.2%), 91 (100); HRMS (EI) *m*/*z* calcd for $C_{23}H_{20}O_4$: 360.1362; found: 360.1369.

4.1.5. 2,3-Dihydro-2,5-dihydroxy-4*H*-chromen-4-one (6). 3-[2,6-Bis(benzyloxy)phenyl]-3-oxopropanal (1.74 g, 4.83 mmol) was dissolved in EtOH (70 mL) and hydrogenated over Pd/C (10%, 670 mg) at 50 psi in a Parr hydrogenation apparatus for 26 h. The solution was filtered through Celite, rinsed with MeOH (50 mL) and EtOAc (50 mL). Removal of the solvent under reduced pressure at room temperature gave a mixture of compounds **6** and **7**, which were separated by column chromatography (petroleum ether/Et_2O, 5:1) yielding 278 mg (33%) of compound **6** and 45 mg (6%) of compound **7**. 2,3-Dihydro-2,5-dihydroxy-4*H*-chromen-4-one (**6**): R_f 0.13 (petroleum ether/EtOAc, 5:1); mp 105–107 °C (103–104 °C)[15]; IR (ν_{max}/cm^{-1}, KBr) 3357, 3059, 1622, 1462, 1330, 1268, 1223, 1110, 1030, 1000, 887, 793, 710; ^{1}H NMR (300 MHz, $CDCl_3$) δ 2.91 (dd, 1H, J = 17.0, 4.0 Hz), 3.09 (dd, 1H, J = 17.0, 3.5 Hz), 3.44 (br s, 1H), 5.87 (br s, 1H), 6.47 (d, 1H, J = 8.5 Hz), 6.58 (d, 1H, J = 8.5 Hz), 7.40 (dd, 1H, J = 8.5, 8.5 Hz), 11.61 (s, 1H); ^{13}C NMR (75 MHz, $CDCl_3$) δ 43.0, 94.4, 107.8, 108.1, 110.2, 138.4, 157.6, 161.7, 196.3; MS (EI, 70 eV, *m*/*z*, (%)) 180 (M$^+$, 62%), 108 (100); HRMS (EI) *m*/*z* calcd for $C_9H_8O_4$: 180.0423; found: 180.0426; Anal. Calcd for $C_9H_8O_4$: C, 60.00; H, 4.48; N, 0; found: C, 60.14; H, 4.37; N, 0. 5-Hydroxy-4*H*-chromen-4-one (**7**): R_f 0.24 (petroleum ether/EtOAc, 5:1); mp 121-125 °C (125.5–127.5 °C)[27]; IR (ν_{max}/cm^{-1}, KBr) 3075, 1661, 1620, 1475, 1427, 1364, 1260, 1217, 1165, 1047, 1001, 837, 797, 741; ^{1}H NMR (300 MHz,

$CDCl_3$) δ 6.31 (d, 1H, J = 6.0 Hz), 6.83 (dd, 1H, J = 8.5, 0.5 Hz), 6.92 (dd, 1H, J = 8.5, 0.5 Hz), 7.55 (dd, 1H, J = 8.5, 8.5 Hz), 7.85 (d, 1H, J = 6.0 Hz), 12.41 (s, 1H); ^{13}C NMR (75 MHz, $CDCl_3$) δ 107.2, 111.5, 111.6, 111.9, 135.5, 156.3, 156.7, 160.9, 183.0; MS (EI, 70 eV, *m*/*z*, (%)) 162 (M^+, 100%); HRMS (EI) *m*/*z* calcd for $C_9H_6O_3$: 160.0317; found: 162.0317.

4.2. Homology modelling

The homology building of 3HNR from *C. lunata* was achieved using the crystal structures of 3HNR from the fungus *M. grisea* (PDB code 1YBV)[16] and of 17β-HSD from the fungus *Cochliobolus lunatus* (17β-HSDcl) as templates.[17] The identities of the amino-acid residues between the modelled sequence and the templates were 74% and 58%, respectively. For the building of the three-dimensional model, the molecular modelling package WHATIF[18] was used, along with the CHARMM programme for macromolecular simulations.[28] After the alignment of the 3HNR sequence from *C. lunata* with each of the templates, all the residues in each of the template structures that differed from those in 3HNR from *C. lunata* were changed, using the BLDPIR command in WHATIF. The two models were relaxed by 20 cycles of the steepest descent (s.d.) refinement with CHARMM. The insertion of two amino acids in both models was achieved manually, and an additional residue originating from the 1YBV template was removed from the model, to obtain the full three-dimensional structural models of 3HNR from *C. lunata*. The missing residues were introduced, using the DGLOOP command in WHATIF, while the redundant residue was deleted and the ends connected by the commands DELETE and PASTE. Each modification was followed by 20 cycles of s.d. refinement with CHARMM. After completing the model, it was put in a cube of water molecules (8124) and subjected to 150 relaxation steps (50 steps of s.d. optimization, 50 steps of optimization by the adopted basis Newton–Raphson method, 50 steps of descent lattice optimization). Subsequently, several iterations of molecular dynamic simulations invoking the EWALD summation for calculating the electrostatic interactions were performed on the model originating from the 1YBV template. They were performed for 100 ps at constant pressure and temperature (CPT, 1 bar, 300 °C, time step 1 fs), with the aim of checking the stability and correctness of the model structure. The less acceptable portions were recognized by the CHECK command in WHATIF, and then remodelled or taken from the corresponding part of the homology model built with the fungal 17β-HSDcl structure as a template. It should be noted here that the NADPH molecule was included in all the optimizations and molecular dynamic simulations.

In parallel calculations, we built and optimized a three-dimensional structure of DDBO via quantum mechanics using MOLDEN, a processing programme of molecular and electronic structure,[29] and the Gaussian 97 electronic structure programme, respectively. For the QM calculation, we used the 6-31g* basis set at the Hartree–Fock level. For the molecular mechanics energy and dynamic calculations, we assigned atomic types for the DDBO molecule using types in the CHARMM distribution C27n1 topology file, and charges calculated according to Mullikan's approximation were applied. Under these conditions, a satisfactory fit to the ab initio energy potentials and geometry was obtained.

In the next step, we manually docked DDBO into the cavity above the C4 atom of the NADPH molecule. The appropriate three atoms of DDBO were superimposed on the corresponding atoms of dihydroxyphenyl-dihydroxy-dihydro chromenone, situated in the active site of grape dihydroflavonol 4-reductase (PDB code 2NNL).[22] The complex structure was now fully relaxed without moving any of the protein and NADPH atoms.

Finally, our three-dimensional model of 3HNR from *C. lunata* with NADPH and docked DDBO was once again put in a cube of water molecules (8124), relaxed and subjected to 500 ps of constant pressure and temperature (CPT) dynamic simulation (1 bar, 300 °C, time step 1 fs), using the EWALD summation for calculating the electrostatic interactions, as described above. The very last step in the building process was a 60-step QMMM refinement of the final frame of the EWALD dynamics simulation, assigning the pyridine ring of NADPH, the side chains of catalytic triad (S149, Y163, K167) and the DDBO molecule using quantum mechanics, whilst the rest of protein and water molecules with H-bond contacts (86 of them) were treated using molecular mechanics.

4.3. Inhibition studies

4.3.1. 3HNR expression and purification. The 3HNR from *C. lunata* was prepared as a glutathione-*S*-transferase (GST)-fusion protein in *E. coli* BL21-AI cells (Invitrogen). It was then purified by affinity binding to Glutathione–Sepharose followed by cleavage with thrombin, as described previously.[30] Protein concentrations were determined according to Bradford[31] with bovine serum albumin as standard. The purity of the 3HNR was checked by SDS–PAGE on 12% polyacrylamide gels, using Coomassie blue staining.[32]

4.3.2. Inhibition assay. Oxidation of the non-physiological substrate 2,3-dihydro-2,5-dihydroxy-4H-benzopyran-4-one (DDBO) to 4,5-dihydroxy-2H-benzopyran-2-one (DBO) with the concomitant reduction of $NADP^+$ to NADPH was followed using a Beckman DU7500 diode array spectrophotometer equipped with a temperature controller accessory (Peltier). The difference in NADPH absorbance was measured at 340 nm and 25 °C.

Structurally different compounds were tested for their inhibitory activities against recombinant 3HNR. The initial rates of the enzymatic reactions in the absence and presence of the compounds being tested were measured at 0.2 μM enzyme, 100 μM substrate and 500 μM coenzyme concentrations. The concentrations of the tested compounds were 100 μM (for screening) and 5 μM to 200 μM (for IC_{50} determination). The

IC_{50} values were determined for the compounds that showed more than 35% inhibition in the screening. Measurements were carried out in 0.6 mL of 100 mM phosphate buffer, pH 7.0, and a 1% final *N*,*N*-dimethylformamide concentration.

4.3.3. Data analysis. At 340 nm, the extinction coefficient for DDBO is $2.42\ mM^{-1}\ cm^{-1}$; for DBO, $0.69\ mM^{-1}\ cm^{-1}$; for NADPH, $6.2\ mM^{-1}\ cm^{-1}$; and for $NADP^+$, $0\ mM^{-1}\ cm^{-1}$. The net $\Delta\varepsilon_{340}$ for the oxidation of DDBO by $NADP^+$ catalyzed by 3HNR is $4.5\ mM^{-1}\ cm^{-1}$.[15] Thus, a molar extinction coefficient of $4.5\ mM^{-1}\ cm^{-1}$ was used to calculate the initial velocities. The percentage inhibition was given by $100 - [(v_i\ (\text{with inhibitor})/v_0\ (\text{without inhibitor})) \times 100]$. The IC_{50} values were determined graphically from a plot of $\log_{10}$ (inhibitor concentration) versus percentage inhibition using the GraphPad Prism Version 4.00 programme (GraphPad Software, Inc.).

4.4. Molecular docking

Automated docking was used to predict the binding orientation of inhibitors within the active site of 3HNR from *C. lunata*. The genetic algorithm method implemented in the programme AutoDock 3.0 was used.[33] The structures of inhibitors were prepared using HyperChem 7.5 (HyperChem, version 7.5 for Windows. Hypercube, Inc.: Gainesville, FL, 2002). The ligand was removed from the homology built model (see Section 4.2) and polar hydrogen atoms were added, and Kollman charges,[34] atomic solvation parameters and fragmental volumes were assigned to the protein using AutoDock Tools (ADT). For docking calculations, Gasteiger–Marsili partial charges[35] were assigned to the coenzyme molecule, and the ligands and non-polar hydrogen atoms were merged. All the torsions were allowed to rotate during docking. The grid map was generated with the auxiliary programme AutoGrid. The grid dimensions were large enough to cover the inhibitors and the enzyme active site. Lennard-Jones parameters 12–10 and 12–6, supplied with the programme, were used for modelling H-bonds and van der Waals interactions, respectively. The distance-dependent dielectric permittivity of Mehler and Solmajer was used for calculation of the electrostatic grid maps.[36] For all ligands, random starting points, orientations and torsions were used. The translation, quaternion and torsion steps were taken from the default values in AutoDock. The Lamarckian genetic algorithm and the pseudo-Soils and Wets methods were applied for minimization, using the default parameters. The number of docking runs was 250, the population in the genetic algorithm was 250, the number of energy evaluations was 500,000, and the maximum number of iterations was 27,000.

Acknowledgments

This work was supported financially by the Ministry of Education, Science and Sport of the Republic of Slovenia. The authors thank Dr. Chris Berrie for critical reading of the manuscript.

References and notes

1. Revankar, S. G. *Expert Rev. Anti Infect. Ther.* **2005**, *3*, 601.
2. Brandt, M. E.; Warnock, D. W. *J. Chemother.* **2003**, *15*, 36.
3. Wilhelmus, K. R.; Jones, D. B. *Tr. Am. Ophth. Soc.* **2001**, *99*, 111.
4. Revankar, S. G.; Patterson, J. E.; Sutton, D. A.; Pullen, R.; Rinaldi, M. G. *Clin. Infect. Dis.* **2002**, *34*, 467.
5. Polak, A. *Mycoses* **1989**, *33*, 215.
6. Nosanchuck, J. D.; Casadevall, A. *Antimicrob. Agents Chemother.* **2006**, *50*, 3519.
7. Bell, A. A.; Wheeler, M. H. *Ann. Rev. Phytopathol.* **1986**, *24*, 411.
8. Jordan, D. B.; Basarab, G. S.; Liao, D. I.; Johnson, W. M. P.; Winzenberg, K. N.; Winkler, D. A. *J. Mol. Graphics Modell.* **2001**, *19*, 434.
9. Liao, D. I.; Basarab, G. S.; Gatenby, A. A.; Valent, B.; Jordan, D. B. *Structure* **2001**, *9*, 19.
10. Howard, R. J.; Valent, B. *Annu. Rev. Microbiol.* **1996**, *50*, 491.
11. Tsuji, G.; Takeda, T.; Furusawa, I.; Horino, O.; Kubo, Y. *Pestic. Biochem. Physiol.* **1997**, *57*, 211.
12. www.doctorfungus.org. May 2007.
13. Rinaldi, M. G.; Phillips, P.; Schwartz, J. G.; Winn, R. E.; Holt, G. R.; Shagets, F. W.; Elrod, J.; Nishioka, G.; Aufdemorte, T. B. *Diagn. Microbiol. Infect. Dis.* **1987**, *6*, 27.
14. Lanišnik Rižner, T.; Wheeler, M. H. *Can. J. Microbiol.* **2003**, *49*, 110.
15. Thompson, J. E.; Basarab, G. S.; Pierce, J.; Hodge, C. N.; Jordan, D. B. *Anal. Biochem.* **1998**, *256*, 1.
16. Anderson, A.; Jordan, D.; Schneider, G.; Lindquist, Y. *Structure* **1996**, *4*, 1161.
17. Cassetta, A.; Bűdefeld, T.; Lanišnik Rižner, T.; Kristan, K.; Stojan, J.; Lamba, D. *Acta Cryst.* **2005**, *61*, 1032.
18. Vriend, G. *J. Mol. Graph. Model.* **1990**, *8*, 52.
19. McGovern, S. L.; Shoichet, B. K. *J. Med. Chem.* **2003**, *46*, 2895.
20. Jacobson, M. P.; Sali, A. *Annu. Rep. Med. Chem.* **2004**, *39*, 259.
21. Kenyon, V.; Chorny, I.; Carvajal, W. J.; Holman, T. R.; Jacobson, M. P. *J. Med. Chem.* **2006**, *49*, 1356.
22. Petit, P.; Langlois D'Estaintot, B.; Grainer, T.; Gallois, B. *J. Mol. Biol.* **2007**, *368*, 1345.
23. Liao, D. I.; Thompson, J. E.; Fahnestock, S.; Valent, B.; Jordan, D. B. *Biochemistry* **2001**, *40*, 8696.
24. Anderluh, M.; Marc, G.; Sollner Dolenc, M. *Synth. Commun.* **2005**, *35*, 1461.
25. Wilson, B. J. *J. Chem. Soc.* **1939**, 1922.
26. Tsujihara, K.; Hongu, M.; Inamasu, M.; Arakawa, K.; Oku, A.; Matsumoto, M. *Chem. Pharm. Bull.* **1996**, *44*, 1174.
27. Borchardt, T.; Huber, J. A. *J. Med. Chem.* **1975**, *18*, 120.
28. Brooks, B. R.; Bruccoleri, R. E.; Olafson, B. D.; States, D. J.; Swaminanthan, S.; Karplus, M. *J. Comput. Chem.* **1983**, *4*, 187.
29. Schaftenaar, G.; Noordik, J. H. *J. Comput. Aided Mol. Des.* **2000**, *14*, 123.
30. Lanišnik Rižner, T.; Moeller, G.; Thole, H. H.; Žakelj Mavrič, M.; Adamski, J. *Biochem. J.* **1995**, *337*, 425.

31. Bradford, M. M. *Anal. Biochem.* **1976**, *72*, 248.
32. Laemmli, U. K. *Nature* **1970**, *227*, 680.
33. Morris, G. M.; Goodsell, D. S.; Halliday, R. S.; Huey, R.; Hart, W. E.; Belew, R. K.; Olson, A. J. *J. Comput. Chem.* **1998**, *19*, 1639.
34. Weiner, S. J.; Kollman, P. A.; Case, D. A.; Singh, U. C.; Ghio, C.; Alagona, G.; Profeta, S.; Weiner, P. *J. Am. Chem. Soc.* **1984**, *106*, 765.
35. Gasteiger, J.; Marsili, M. *Tetrahedron* **1980**, *36*, 3219.
36. Mehler, E. L.; Solmajer, T. *Protein Eng.* **1991**, *4*, 903.